Supporting information

Effect of Surface Chemistry and Associated Protein Corona on the Long-Term Biodegradation of Iron Oxide Nanoparticles *In Vivo*

Grazyna Stepien,[1,#] María Moros,[1,2,#,] Marta Pérez-Hernández,[1,3] Marta Monge,[4,5] Lucía Gutiérrez,[1] Raluca M. Fratila,[6] Marcelo de las Heras,[7] Sebastián Menao Guillén,[8] Juan José Puente Lanzarote,[8] Conxita Solans,[4] Julian Pardo,[1,3,9] and Jesús Martínez de la Fuente.[6,10,*]*

1-Institute of Nanoscience of Aragon (INA), University of Zaragoza, 50018 Zaragoza, Spain

2- Institute of Applied Sciences and Intelligent Systems-CNR, Via Campi Flegrei, 34, 80078, Pozzuoli, Italy

3- Aragón Health Research Institute (IIS Aragón), Biomedical Research Centre of Aragón (CIBA), 50009 Zaragoza, Spain

4- Institute of Advanced Chemistry of Catalonia (IQAC-CSIC) and CIBER in Bioengineering, Biomaterials and Nanomedicine (CIBER-BBN), Jordi Girona 18-26, Barcelona 08034

5- Department of Pharmacy and Pharmaceutical Technology and Physical Chemistry, University of Barcelona, Av/Joan XXIII s/n, 08028 Barcelona, Spain

6- Aragon Materials Science Institute (ICMA), CSIC-University of Zaragoza and CIBER-BBN, C/Pedro Cerbuna 12, 50009 Zaragoza, Spain

7-Department of Animal Pathology, Veterinary Faculty, University of Zaragoza, 50009 Zaragoza, Spain

8-Department of Clinical Biochemistry. H.C.U. Lozano Blesa, Zaragoza 50009, Spain.

9- ARAID foundation, 50018 Zaragoza, Spain

10-Institute of NanoBiomedicine and Engineering, Shanghai Jiao Tong University, Dongchuan Road 800, 200240 Shanghai, PR China

[#] Equal contribution
* Corresponding authors

IONPs synthesis and functionalization

Monodisperse iron oxide NPs of 11.6 ± 1.3 nm diameter were synthesized following the seed-mediated growth protocol described by Sun et al.[1] First, 7.8 ± 0.7 nm NP seeds were synthesized by mixing and stirring under a flow of argon Iron (III) acetylacetonate $Fe(acac)_3$ (1 eq, 2.01 mmol, 0.71 g), 1,2-hexadecanediol (4.5 eq, 9.98 mmol, 2.58 g), oleic acid (2.8 eq, 5.65 mmol, 1.774 g) and oleylamine (2.1 eq, 4.22 mmol, 1.626 g) solubilized in 40 mL benzyl ether (50 mM with respect to $Fe(acac)_3$). The mixture was heated to 200 °C (at a heating rate of 180 °C/h), maintained at 200 ºC for 2 h and then heated to reflux (305 ºC, heating speed 10 ºC/min) and maintained for 1 h. After cooling down the NPs, they were subsequently washed four times with ethanol, and re-dispersed in hexane. These NPs were used as seeds to obtain 12 nm NPs by mixing and stirring under a flow of argon the following chemicals: $Fe(acac)_3$ (1 eq, 4.02 mmol, 1.42 g), 1,2-hexadecanediol (4.5 eq, 19.97 mmol, 5.16 g), oleic acid (0.7 eq, 3.12 mmol, 0.881 g), oleylamine (0.5 eq, 3.06 mmol, 0.818 g) and 7 nm NPs seeds (40 mg Fe) solubilized in benzyl ether (100 mM with respect to $Fe(acac)_3$). The mixture was heated up to 100 °C for 30 min to evaporate the excess hexane from the seeds (heating rate 180 ºC/h), then to 200 ºC (heating rate 3 ºC/min), maintained at 200 ºC for 1 h and finally heated at reflux (305 ºC, heating rate 7 ºC/min) and maintained for 1 h. The mixture was washed as before. The transfer into water was performed using a modified protocol based on a previously reported method.[2] Briefly, 280 mg of poly(maleic anhydride-alt-1-octadecene); PMAO (MW 30000–50000 Da) were added to a flask containing 200 mL of chloroform and placed in an ultrasonic bath.

Twenty milligrams of NPs diluted in $CHCl_3$ were added drop-wise and the mixture was left in the ultrasonic bath for further 15 min. The solvent was slowly removed under vacuum and 15 mL of 0.1 M NaOH was added to transfer the MNPs to the aqueous phase. To remove the excess of unbound polymer, the solution was centrifuged at 75600 × g for 2 h fourfold.

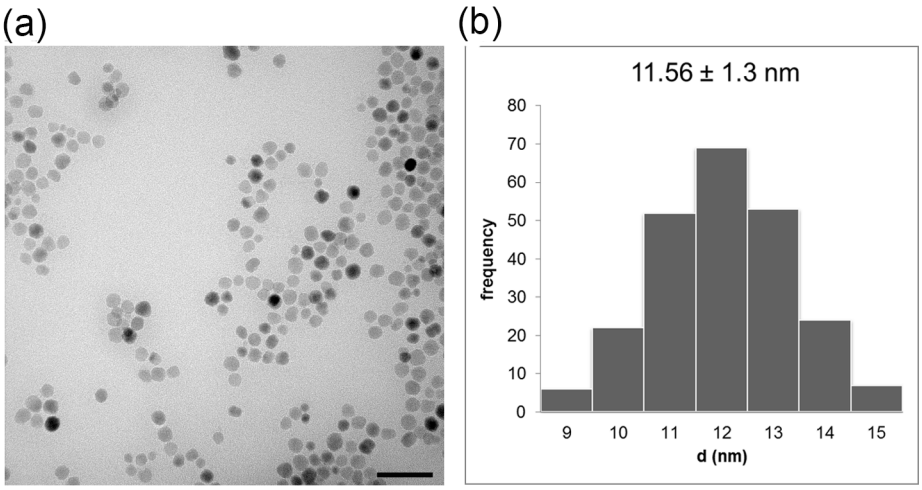

Figure S1. (a) TEM image and (b) histogram of NPs in hexane, obtained after thermal decomposition of Fe(III) acetylacetonate, with a mean diameter of around 12 nm. Scale bar: 50 nm.

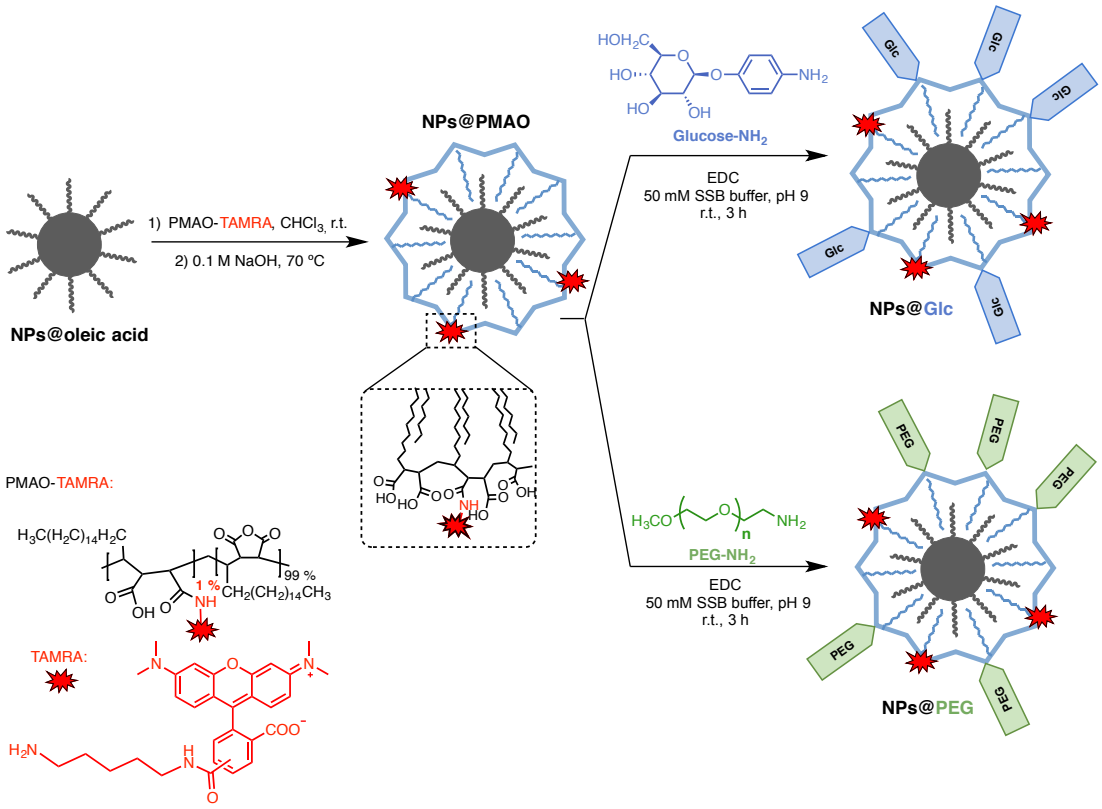

Scheme S1. Strategy of transferring into water 12 nm NPs with the use of TAMRA-modified PMAO polymer. NPs@PMAO were employed for further functionalization with either amine-modified glucose or PEG molecules to obtain NPs@Glc and NPs@PEG, respectively.

NPs characterization

NPs were characterized using transmission electron microscopy (TEM Tecnai T20, OR, USA). Dynamic light scattering and zeta-potential (ζ-potential) measurements were performed in water, combining ten runs per measurement on a Malvern Zetasizer Nano- ZS instrument at 25 °C. Iron was quantified using a standard colorimetric procedure already reported.[3] Briefly, the samples were incubated with aqua regia for 15 min at 60 °C after which Milli-Q water was added to a final volume of 500 µL. 50 µL of the total volume of each solution were transferred to a 96 well plate and KOH and 4,5-dihydroxy-1,3-benzenedisulfonic acid disodium salt monohydrate were subsequently added to a final concentration of 0.9 N and 12 mM, respectively. Finally, 0.2 M sodium phosphate buffer pH 9.7 was added to a final volume of 210 µL and the solution was left at room temperature for 15 min. After this time, sample absorbance at 480 nm was measured on a Thermo Scientific Multiskan™ GO UV/Vis microplate spectrophotometer (MA, USA).

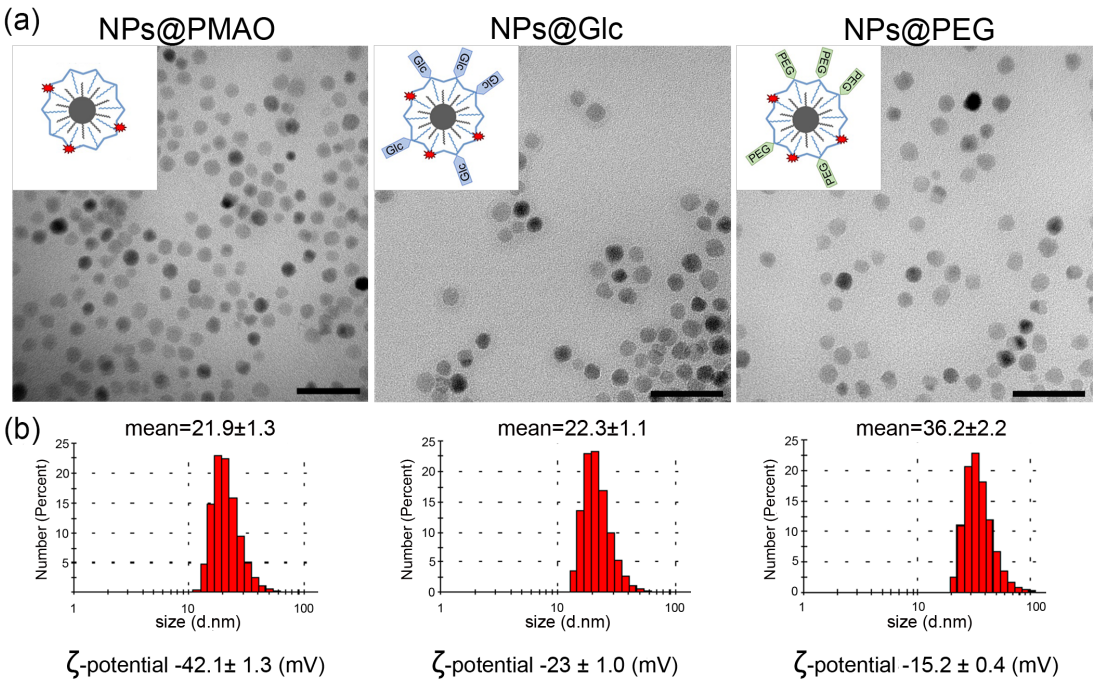

Figure S2. Characterization of NPs@PMAO, NPs@Glc and NPs@PEG by (a) TEM, (b) DLS and ζ-potential. (a) TEM images demonstrate that all NPs share the same size and shape (scale bar: 50 nm). In the left upper corner a schematic diagram of each NP can be found. Readers are referred to Scheme S1 for further information. (b) DLS measurements show that all three NPs types presented narrow size distribution. Reduction in the surface charge of NPs@Glc and NPs@PEG in respect to NPs@PMAO confirms the functionalization of those NPs

- **Evaluation of NPs stability**

Stability of all three NPs types was evaluated performing DLS measurements after the incubation of the NPs in water, PBS or DMEM supplemented with 10% bovine serum for 0, 24 or 48 hours. Each sample was measured three times, combining 10 runs *per* measurement at 25 ºC.

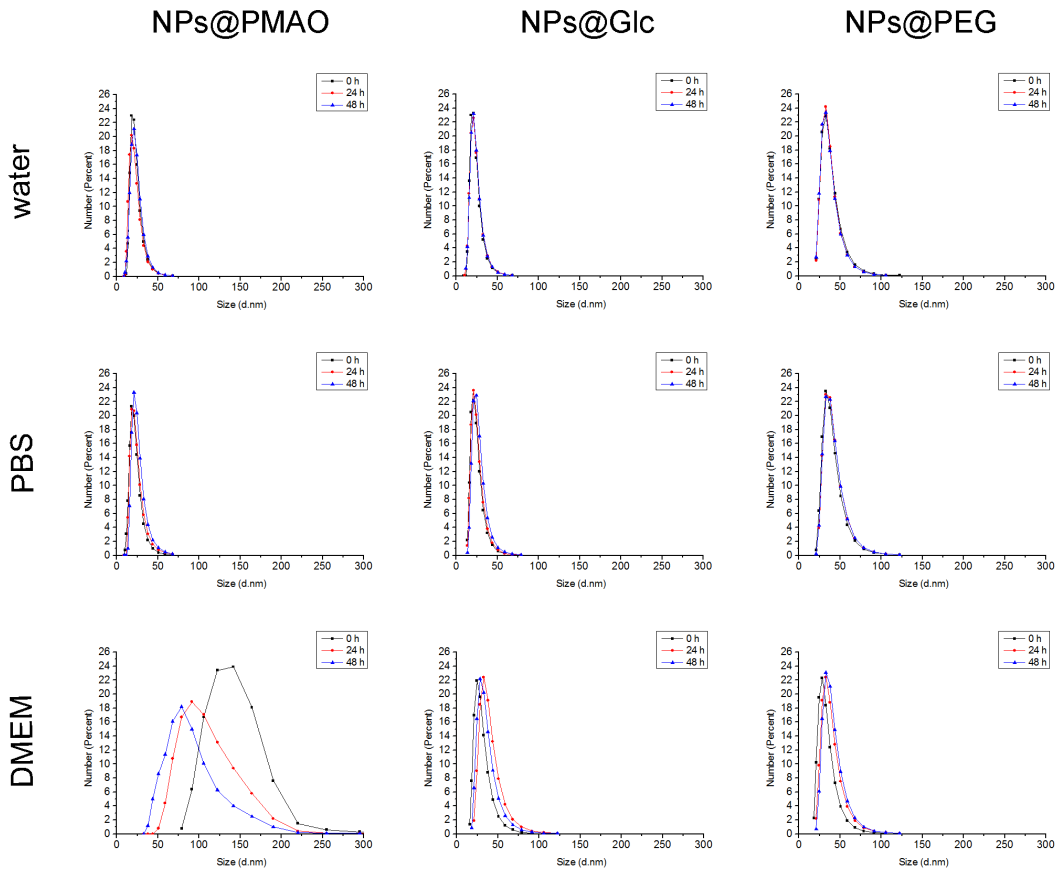

Figure S3. Stability of NPs@PMAO, NPs@Glc and NPs@PEG incubated in water, PBS and complete DMEM (supplemented with 10% bovine serum) measured at three time points: 0, 24 and 48 h. Both functionalized NPs, NPs@Glc and NPs@PEG are stable in all tested mediums up to 48 h, whereas NPs@PMAO aggregate immediately in DMEM as an increment of hydrodynamic diameter is observed.

- **Protein Corona study**

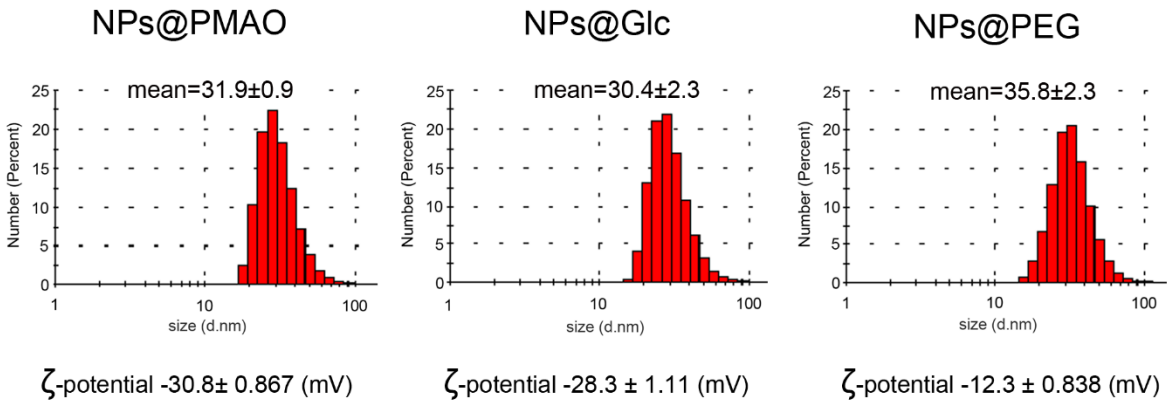

Figure S4. Characterization of NPs@PMAO, NPs@Glc and NPs@PEG after the formation of the PC. A slight increase in the hydrodynamic diameter and a change in zeta potential were observed for all three NPs types of NPs, in respect to their counterparts without PC (Figure S2b).

Protein corona quantification

To proceed with quantification of the amount of protein bound by the nanoparticles, Bicinchoninic Acid (BCA)-assay was used. Briefly, BCA working reagent was prepared by mixing 50 vol of BCA stock solution (Bichinconinic acid, sodium carbonate, sodium tartrate and sodium bicarbonate in 0.1 N NaOH, pH 11.25) with 1 vol of 4 % $CuSO_4 \cdot 5H_2O$ solution prior to beginning the assay. BSA protein standard (0 µg μL^{-1} to 1 µg μL^{-1}) and samples were analyzed in triplicates. 25 µL protein samples were mixed with 200 µL BCA Working Reagent and were incubated at 60 °C for 15 min before reading at 562 nm.

Table S1. Number of proteins and peptides bound to each type of NPs identified by LS-MS/MS.

	Sample	Proteins	Peptides
A	NPs@PMAO	272	2755
B	NP@PEG	284	2664
C	NP@Glc	305	3101

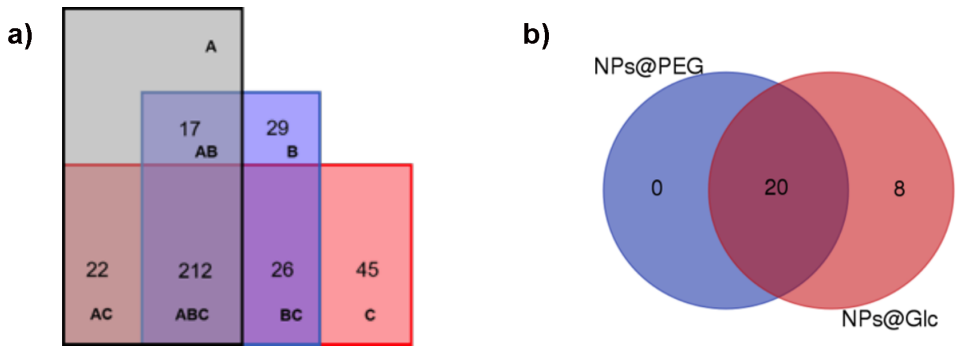

Figure S5. a) Diagram distribution of the 372 different proteins identified, showing the overlapping detected. The specific bound proteins to each type of NPs are represented with pure colors: A-NPs@PMAO, B-NPs@PEG, and C- NPs@Glc, whereas: AB- represents proteins common for NP@PMAO and NPs@PEG; AC- represents proteins common for NP@PMAO and NPs@Glc; BC-

represents proteins common for NP@PEG and NPs@Glc; ABC- represents proteins common for all three NPs type. **b)** Venn diagram corresponding to the molecular and cellular function analysis from NPs@PEG and NPs@Glc samples generated by the Ingenuity pathway analysis software (Table S5).

Table S2. Specific bound proteins identified on the surface of NPs@PMAO

Accession[a]	**Name**	**Score**[b]	**Peptides**[c]	**SC [%]**[d]	**RMS90 [ppm]**[e]
A5PJE3_BOVIN	Fibrinogen alpha chain	548,9	13	22,60	0,70
TBA4A_BOVIN	Tubulin alpha-4A chain	195,9	4	12,90	208,93
A6QLB7_BOVIN	Adenylyl cyclase-associated protein	111,7	3	10,80	4,21
A0A0F7RPX0_BOVIN	Macrophage migration inhibitory factor	75,6	2	17,40	1,07
ENPP2_BOVIN	Ectonucleotide pyrophosphatase/phosphodiesterase family member 2	74,3	3	5,50	3,52
EF1A1_BOVIN	Elongation factor 1-alpha 1	59,2	2	11,30	1,56
F1N1W3_BOVIN	Thrombospondin-2	59,1	2	1,60	0,67
TRFL_BOVIN	Lactotransferrin	53,2	2	2,30	0,83
LDHB_BOVIN	L-lactate dehydrogenase B chain	48,2	2	7,50	1,13
TBB4A_BOVIN	Tubulin beta-4A chain	46,0	2	9,50	3,85
COTL1_BOVIN	Coactosin-like protein	45,1	1	11,30	2,34
PYGL_BOVIN	Glycogen phosphorylase, liver form	43,6	1	1,60	614,55
E1B7G5_BOVIN	Uncharacterized protein	42,7	1	0,70	0,31
NUCB1_BOVIN	Nucleobindin-1	41,7	1	3,40	0,20
G3N2H5_BOVIN	Protein S100 (Fragment)	30,3	1	25,50	3,08
B4GA1_BOVIN	Beta-1,4-glucuronyltransferase 1	28,2	1	6,70	6,75
E1B9R5_BOVIN	Uncharacterized protein	27,7	1	0,10	0,77
ORC4_BOVIN	Origin recognition complex subunit 4	26,8	1	3,40	3,39
F1MZX6_BOVIN	Uncharacterized protein	26,6	1	0,50	0,98
Q08DQ6_BOVIN	Uncharacterized protein	26,2	1	2,00	0,85
Q08DR4_BOVIN	UDP-glucose ceramide glucosyltransferase	26,2	1	1,50	0,55

[a] accession: a unique identifier given to a biological polymer sequence (protein) when it is submitted to a sequence data base

[b] score: number which reflects the combined scores of all observed mass spectra that can be matched to amino acid sequences within that protein. A higher score indicates a more confident match

[c] peptides: number of peptides detected for each protein identified

[d] SC (%): percentage of the database protein sequence covered by matching peptides

[e] RMS90 [ppm]: mass accuracy of generated data.

Table S3. Specific bound proteins identified on the surface of NPs@Glc

Accession[a]	**Name**	**Score**[b]	**Peptides**[c]	**SC [%]**[d]	**RMS90 [ppm]**[e]
F1MMK9_BOVIN	Protein AMBP	999,5	14	40,30	1,26
F1MUT4_BOVIN	Coagulation factor XI	631,6	18	44,50	0,67
FIBB_BOVIN	Fibrinogen beta chain	377,1	12	30,10	1,34
Q1RMN9_BOVIN	C4b-binding protein alpha-like	305,7	7	46,40	0,27
PROF1_BOVIN	Profilin-1	124,0	4	32,90	1,53
G3MY71_BOVIN	Uncharacterized protein (Fragment)	107,5	1	15,00	2,07
G5E604_BOVIN	Uncharacterized protein (Fragment)	93,0	1	15,00	3,88
S10AC_BOVIN	Protein S100-A12	90,2	3	58,70	187,01
TBB4B_BOVIN	Tubulin beta-4B chain	87,5	3	17,10	1,16
G1K1A3_BOVIN	Nucleoside diphosphate kinase (Fragment)	82,5	2	20,90	1,81
F1MXR3_BOVIN	Uncharacterized protein	77,2	2	3,30	0,97
A5D7L1_BOVIN	CLEC11A protein	76,4	2	5,90	1,39
ALDOB_BOVIN	Fructose-bisphosphate aldolase B	73,5	2	9,10	1,96
F1MPD1_BOVIN	Uncharacterized protein (Fragment)	72,8	1	0,90	0,34
CTHL4_BOVIN	Cathelicidin-4	70,9	1	11,10	3,02
F1MPP2_BOVIN	Uncharacterized protein	68,0	2	9,90	1,96
BLVRB_BOVIN	Flavin reductase (NADPH)	63,9	1	10,20	3,91
F1N401_BOVIN	Collagen alpha-1(XII) chain	63,3	2	1,00	585,81
E1B9H5_BOVIN	Uncharacterized protein	60,4	1	1,40	0,93
F1MRZ8_BOVIN	Uncharacterized protein	54,7	1	4,00	2,52
TIMP1_BOVIN	Metalloproteinase inhibitor 1	52,8	1	9,70	1,02
F1N3V0_BOVIN	Malic enzyme	48,3	1	1,80	1,54
DDBX_BOVIN	Dihydrodiol dehydrogenase 3	44,2	1	5,90	0,69
PPIE_BOVIN	Peptidyl-prolyl cis-trans isomerase E	43,9	1	6,60	0,09
BASP1_BOVIN	Brain acid soluble protein 1	43,0	1	6,20	2,62
GLO2_BOVIN	Hydroxyacylglutathione hydrolase, mitochondrial	42,3	2	7,10	1,92

ISK6_BOVIN	Serine protease inhibitor Kazal-type 6	42,2	1	20,00	0,62
ANG1_BOVIN	Angiogenin-1	40,6	2	15,50	0,53
A3KLR9_BOVIN	Superoxide dismutase [Cu-Zn]	39,8	1	5,40	2,73
F1MRZ5_BOVIN	Uncharacterized protein	39,5	1	1,70	8,31
HSP7C_BOVIN	Heat shock cognate 71 kDa protein	37,5	2	3,80	1,50
E1BH94_BOVIN	Uncharacterized protein (Fragment)	35,5	1	6,10	291,07
E1BF01_BOVIN	Uncharacterized protein	33,3	1	0,40	0,20
IBP3_BOVIN	Insulin-like growth factor-binding protein 3	31,8	1	2,70	0,71
PRDX2_BOVIN	Peroxiredoxin-2	30,8	1	9,00	1,81
VASP_BOVIN	Vasodilator-stimulated phosphoprotein	30,5	1	2,30	0,50
MPRI_BOVIN	Cation-independent mannose-6-phosphate receptor	30,3	1	0,40	1,36
F1MS67_BOVIN	Uncharacterized protein	29,8	1	0,60	1076,73
A6QLN7_BOVIN	Dimethylaniline monooxygenase [N-oxide-forming]	29,3	2	2,60	1,54
F1N169_BOVIN	Uncharacterized protein	28,1	1	0,60	3,20
FGL2_BOVIN	Fibroleukin	27,6	1	1,80	0,35
MBL2_BOVIN	Mannose-binding protein C	27,6	1	3,60	2,22
F1MKN3_BOVIN	28S ribosomal protein S34, mitochondrial	25,7	1	3,20	0,24
G3N0B5_BOVIN	Uncharacterized protein	25,6	1	5,40	6,59
FGL1_BOVIN	Fibrinogen-like protein 1	25,5	1	2,90	0,82

[a] accession: a unique identifier given to a biological polymer sequence (protein) when it is submitted to a sequence data base

[b] score: number which reflects the combined scores of all observed mass spectra that can be matched to amino acid sequences within that protein. A higher score indicates a more confident match

[c] peptides: number of peptides detected for each protein identified

[d] SC (%): percentage of the database protein sequence covered by matching peptides

[e] RMS90 [ppm]: mass accuracy of generated data.

Table S4. Specific bound proteins identified on the surface of NPs@PEG

Accession[a]	Name	Score[b]	Peptides[c]	SC [%] [d]	RMS90 [ppm][e]
E1BFN5_BOVIN	Uncharacterized protein	758,1	13	22,00	2,01
ACTA_BOVIN	Actin, aortic smooth muscle	325,6	7	19,90	2,49
K1C10_BOVIN	Keratin, type I cytoskeletal 10	298,1	9	14,10	0,65
K2C7_BOVIN	Keratin, type II cytoskeletal 7	228,3	3	6,40	0,94
F1MFW9_BOVIN	Uncharacterized protein (Fragment)	217,2	3	6,70	2,50
LYSC_BOVIN	Lysozyme C	113,4	2	22,40	1,90
Q3ZBY4_BOVIN	Fructose-bisphosphate aldolase	70,1	1	6,30	1,28
LDHA_BOVIN	L-lactate dehydrogenase A chain	61,6	2	6,60	1,01
E1B9V3_BOVIN	Phospholipase A(2)	60,3	1	8,80	1,94
G1K238_BOVIN	Collagen alpha-1(IV) chain	58,1	1	0,90	0,93
RS27A_BOVIN	Ubiquitin-40S ribosomal protein S27a	56,1	2	16,00	0,99
G3N269_BOVIN	Fatty acid-binding protein, epidermal	52,0	1	6,70	0,01
E1BIR8_BOVIN	Uncharacterized protein	43,0	1	0,30	0,84
G3X6S5_BOVIN	SH3 domain-binding glutamic acid-rich-like protein 3	38,2	1	5,60	0,37
E1BJB1_BOVIN	Uncharacterized protein	37,9	2	9,90	1,89
A2VDR1_BOVIN	RAB40C, member RAS oncogene family	37,3	1	5,70	9,31
KIF3C_BOVIN	Kinesin-like protein KIF3C	34,5	1	0,80	0,56
ZA2G_BOVIN	Zinc-alpha-2-glycoprotein	33,7	1	5,70	2,23
RCN3_BOVIN	Reticulocalbin-3	32,2	1	3,70	0,63
F1MWU2_BOVIN	Uncharacterized protein (Fragment)	31,1	1	1,20	1,48
Q2KJH7_BOVIN	Aldehyde dehydrogenase 18 family, member A1	30,7	1	1,00	0,32
F1MWU9_BOVIN	Uncharacterized protein	30,1	1	1,70	3,73
E1BBC8_BOVIN	Uncharacterized protein	29,6	1	0,80	4,14
Q0VD16_BOVIN	MAP2K1 protein	28,9	1	2,00	0,28
C1K3N7_BOVIN	Thymosin beta 4 X-linked	28,0	1	27,30	3,05
A4IFL4_BOVIN	PPARD protein	27,2	1	1,60	2,51
VWF_BOVIN	von Willebrand factor (Fragment)	27,2	1	2,60	0,18
E1BB21_BOVIN	Desmocollin-3	27,0	1	1,00	1069,44

URP2_BOVIN	Fermitin family homolog 3	26,2	1	1,40	2,88

[a] accession: a unique identifier given to a biological polymer sequence (protein) when it is submitted to a sequence data base

[b] score: number which reflects the combined scores of all observed mass spectra that can be matched to amino acid sequences within that protein. A higher score indicates a more confident match

[c] peptides: number of peptides detected for each protein identified

[d] SC (%): percentage of the database protein sequence covered by matching peptide

Table S5. Molecular and Cellular Function analysis from NPs@PEG and NPs@Glc samples generated by the Ingenuity pathway analysis software.

Sample	**Number**	**Molecular and Cellular Functions**	**NPs@PEG protein Number**	**NPs@Glc protein Number**
NPs@Glc & NPs@PEG	20	Gene Expression	2	2
		Vitamin and Mineral Metabolism	1	2
		Cellular Assembly and Organization	4	10
		Cellular Function and Maintenance	6	12
		Cell Death and Survival	6	20
		Cell-To-Cell Signaling and Interaction	4	21
		Cellular Development	6	16
		Cell Cycle	2	5
		Cellular Growth and Proliferation	4	16
		Cellular Movement	8	19
		Carbohydrate Metabolism	6	9
		Molecular Transport	5	12
		Cellular Compromise	4	4
		Energy Production	2	2
		Small Molecule Biochemistry	7	16
		Cell Morphology	4	18
		Drug Metabolism	1	2
		Lipid Metabolism	5	11
		Amino Acid Metabolism	1	1
		Protein Synthesis	3	11
NPs@Glc	8	Protein Trafficking		6
		Protein Degradation		3
		Nucleic Acid Metabolism		2
		Post-Translational Modification		3
		RNA Damage and Repair		2
		DNA Replication, Recombination, and Repair		2
		Cell Signaling		6
		Free Radical Scavenging		2

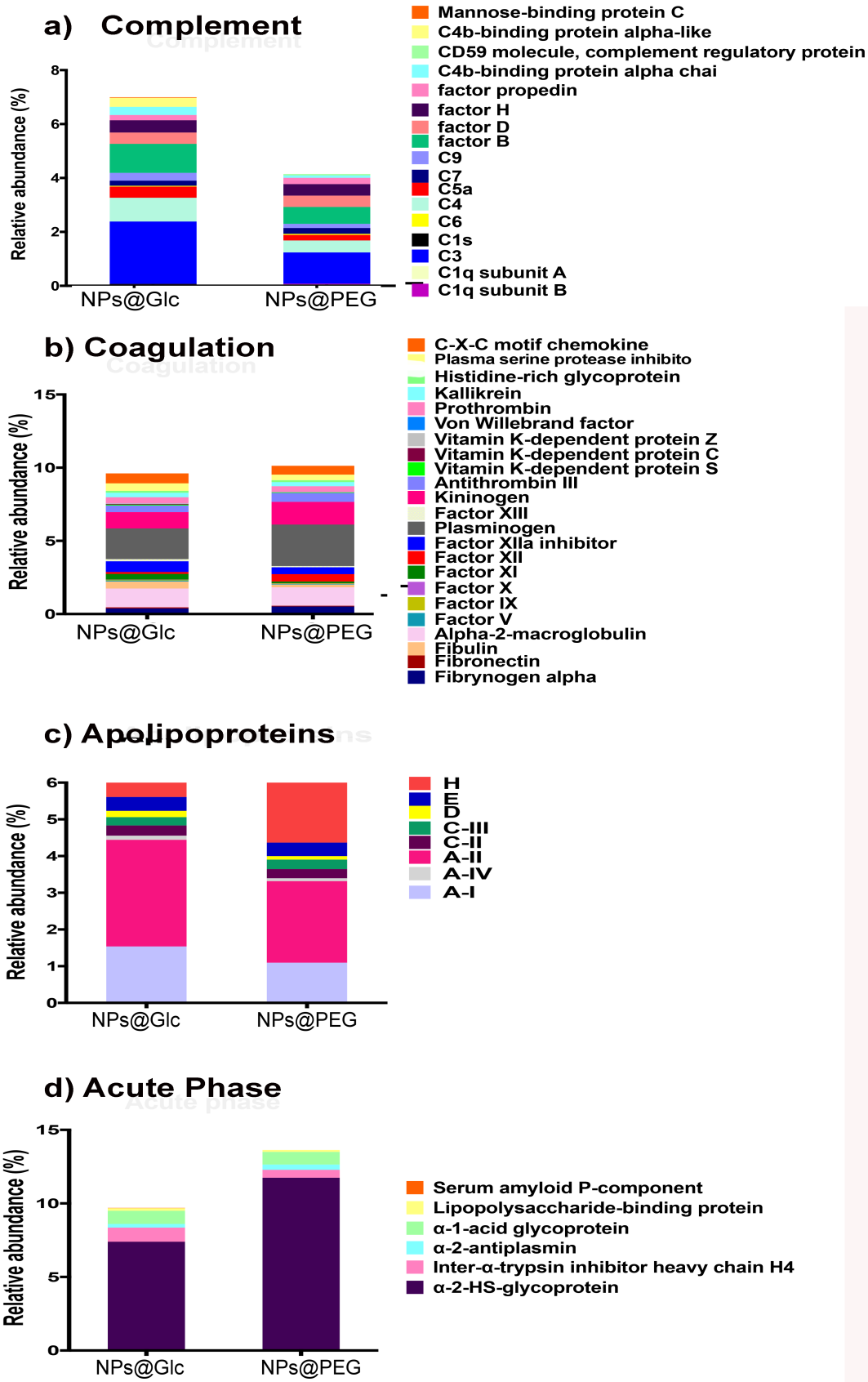

Figure S6. Relative abundance of proteins from (a) complement, (b) coagulation, (c) apolipoproteins and (d) acute phase group, adsorbed on NPs@Glc and NPs@PEG.

- ***In vitro* degradation study of the NPs**

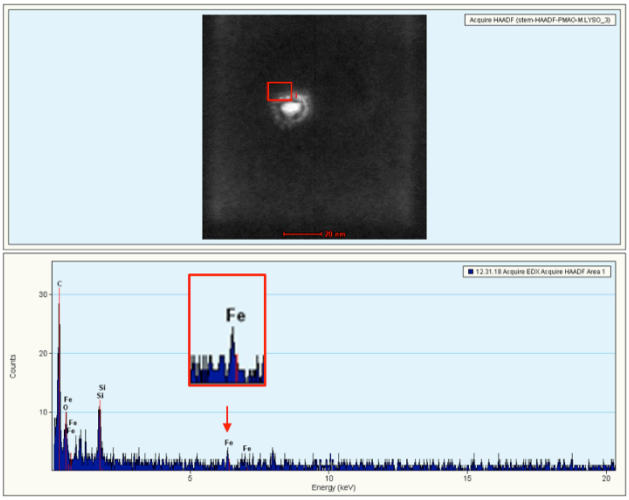

Figure S7. X-Ray Microanalysis of the NPs@PMAO incubated in the lysosomal medium showed that the dissolved iron was retained around NP core and most probably made a complex with the PMAO polymer.

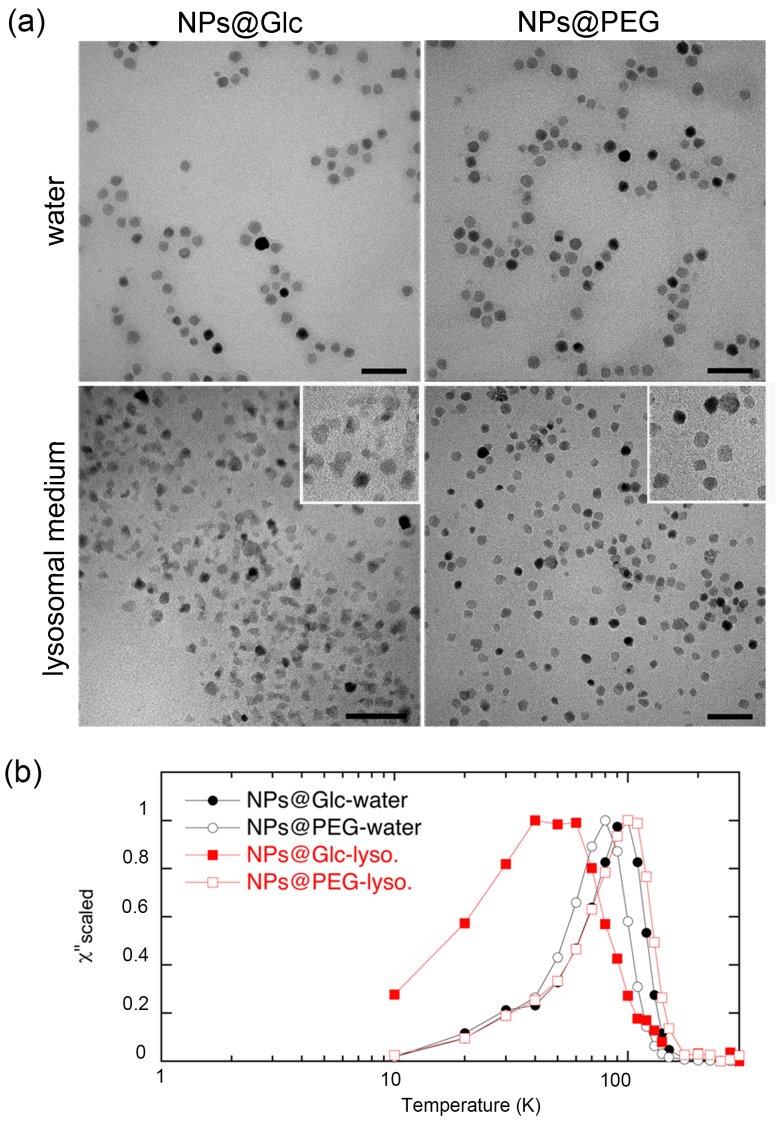

Figure S8. (a) *In vitro* degradation study of NPs@Glc and NPs@PEG. Scale bar: 50 nm. (b) Temperature dependence of the out-of-phase component of the AC magnetic susceptibility from NPs@Glc and NPs@PEG incubated for ten days in the lysosomal medium and water (control).

- **Short and long-term toxicity study**

Recently, a study using PEG-coated gold NPs showed that the toxicity induced by the NPs was different depending on the animal gender.[4] Therefore, the biodistribution and toxicity of the two NPs types were analyzed employing 6-weeks old Swiss male and female mice and repeating the *in vivo* experiments at different times and with different batches of NPs, to assure reproducibility of results. Both NP types showed the same results in terms of toxicity and biodistribution profile for both female and male individuals. Therefore the results presented here correspond only to female animals.

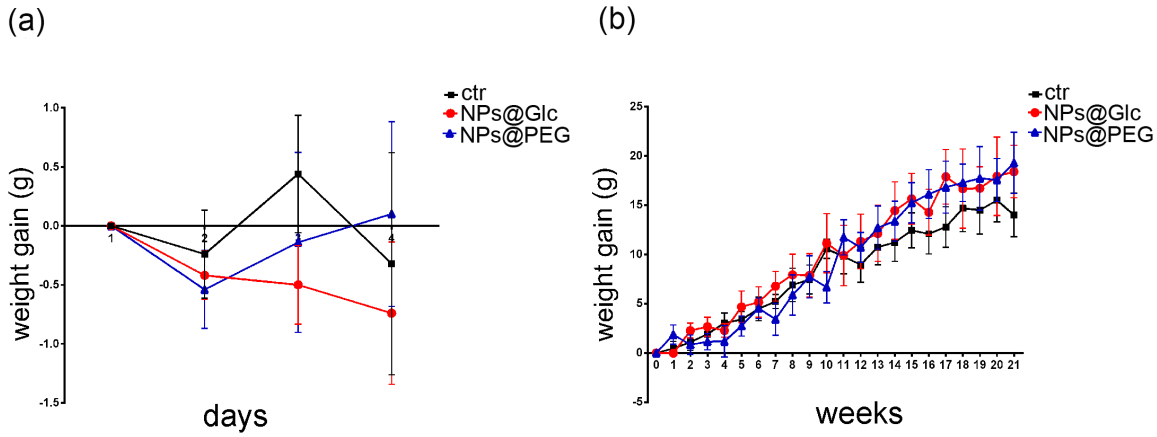

Figure S9. Gain of animal body weight during (a) 72 hours and (b) four months study, after the administration of NPs@Glc, NPs@PEG or PBS in the case of control animals. No statistically significant differences have been found between animals injected with NPs and the control ones (unpaired t-test, $p > 0.05$).

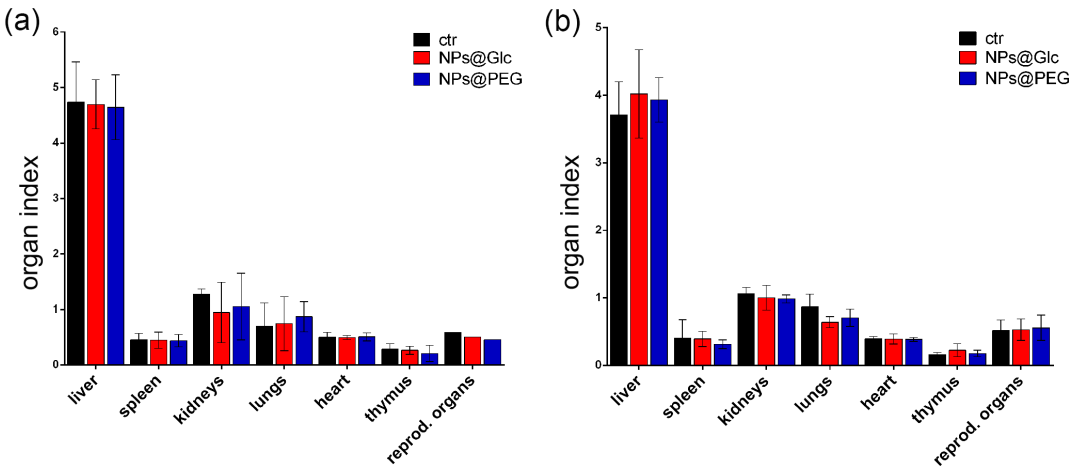

Figure S10. Organ index evaluated (a) 72 h and (b) four months after the administration of NPs@Glc, NPs@PEG or PBS in the case of control animals. No statistically significant differences have been found between animals injected with NPs and the control ones (unpaired t-test, $p > 0.05$).

- **Histology examination of hematoxylin and eosin stained tissue sections**

For pathological examination of the organs, pieces of the excised organs were fixed and processed as described in the section: *Fluorescence microscopy examination of tissue sections.* After dewaxing and hydration process, the samples were stained with hematoxylin (Carazzi's hematoxylin, Panreac; ref 255298) and eosin (Panreac; ref. 131026) and mounted with permanent mounting medium DPX.

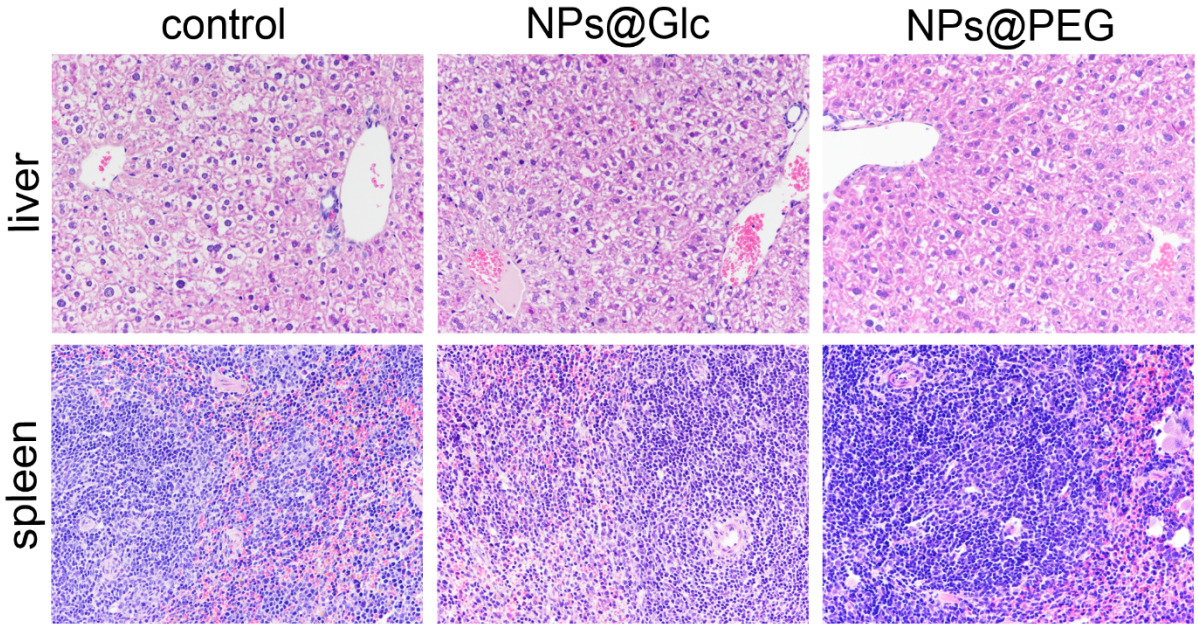

Figure S11. Haematoxylin- eosin (HE) staining of the liver and spleen histological sections evaluated 72 h after NPs administration showed no difference in respect to control animals injected with PBS (20 x magnification).

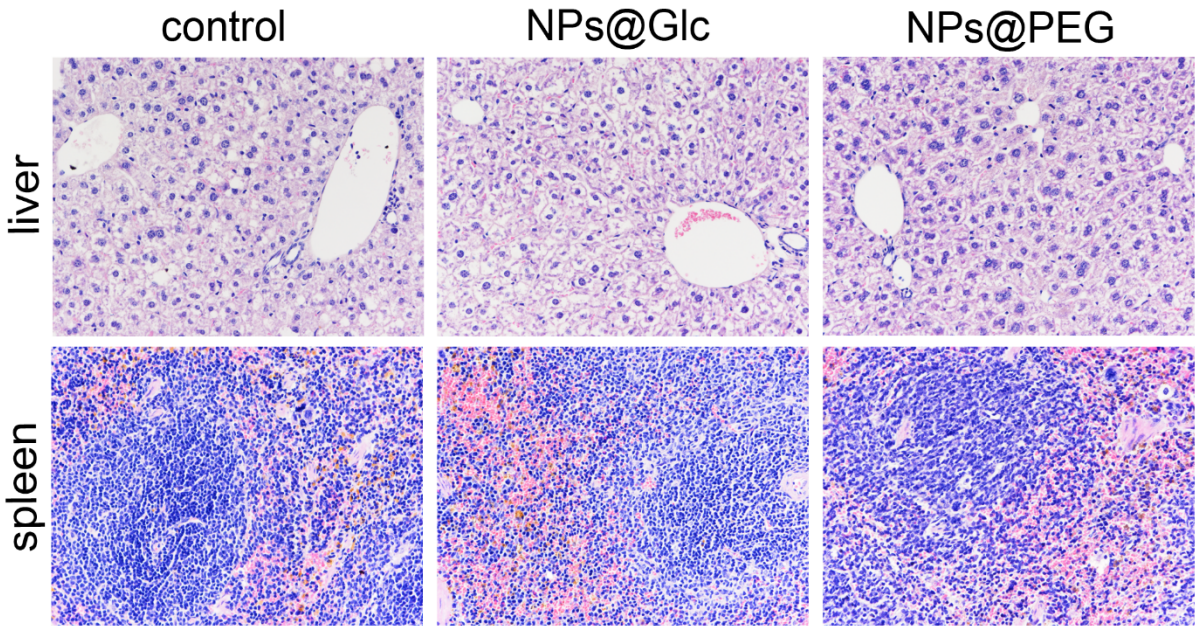

Figure S12. Haematoxylin- eosin (HE) staining of the liver and spleen histological sections evaluated four months after NPs administration showed no difference in respect to control animals injected with PBS (20 x magnification).

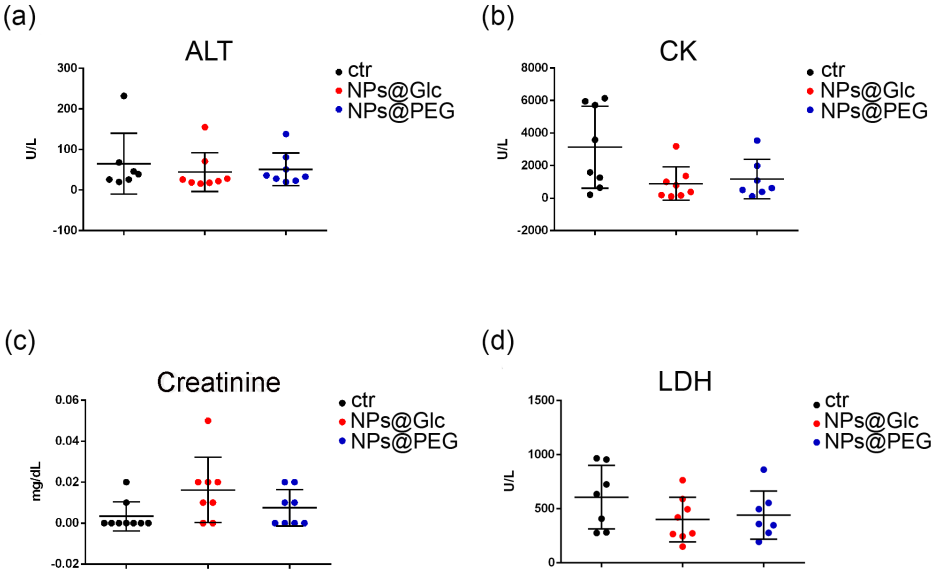

Figure S13. Analysis of blood chemical parameters: (a) alanine aminotransferase (ALT), (b) creatinine kinase (CK), (c) creatinine and (d) lactate dehydrogenase (LDH) performed 72 h after the administration of NPs@Glc, NPs@PEG or PBS in the case of control animals. No statistically significant differences have been found between animals injected with NPs and the control ones (unpaired t-test, $p > 0.05$).

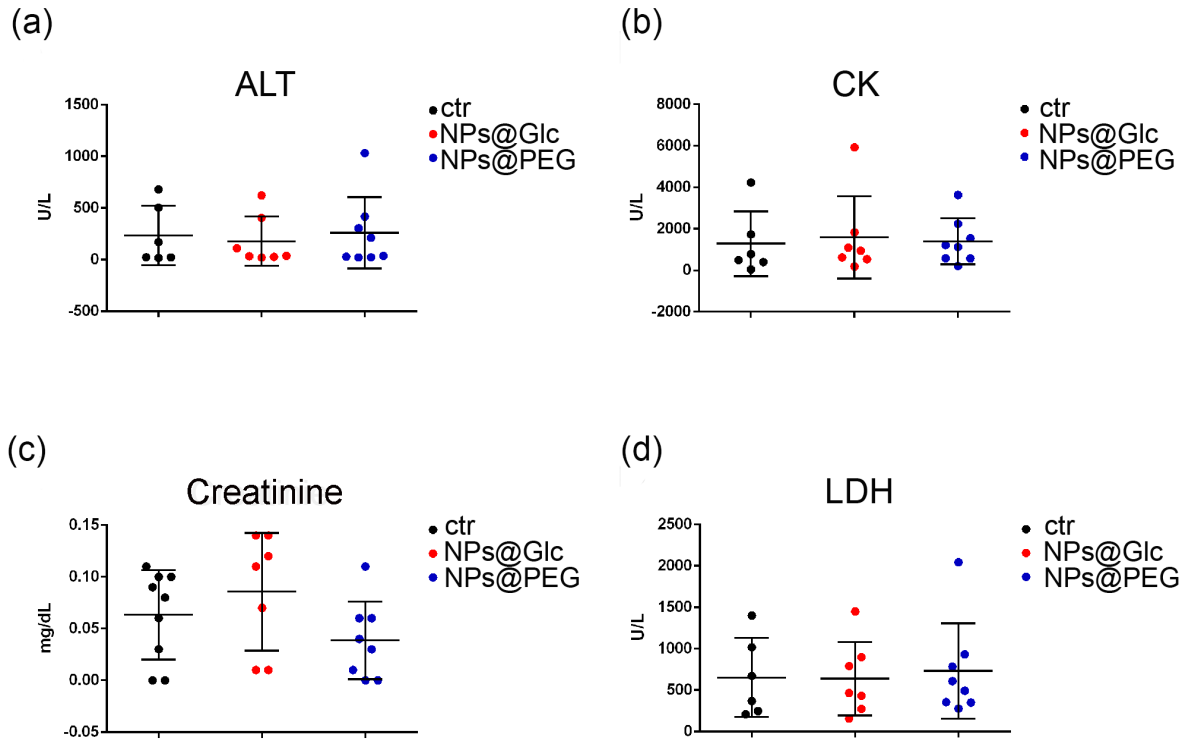

Figure S14. Analysis of blood chemical parameters: (a) alanine aminotransferase (ALT), (b) creatinine kinase (CK), (c) creatinine and (d) lactate dehydrogenase (LDH) performed four months after the administration of NPs@Glc, NPs@PEG or PBS in the case of control animals. No statistically significant differences have been found between animals injected with NPs and the control ones (unpaired t-test, $p > 0.05$).

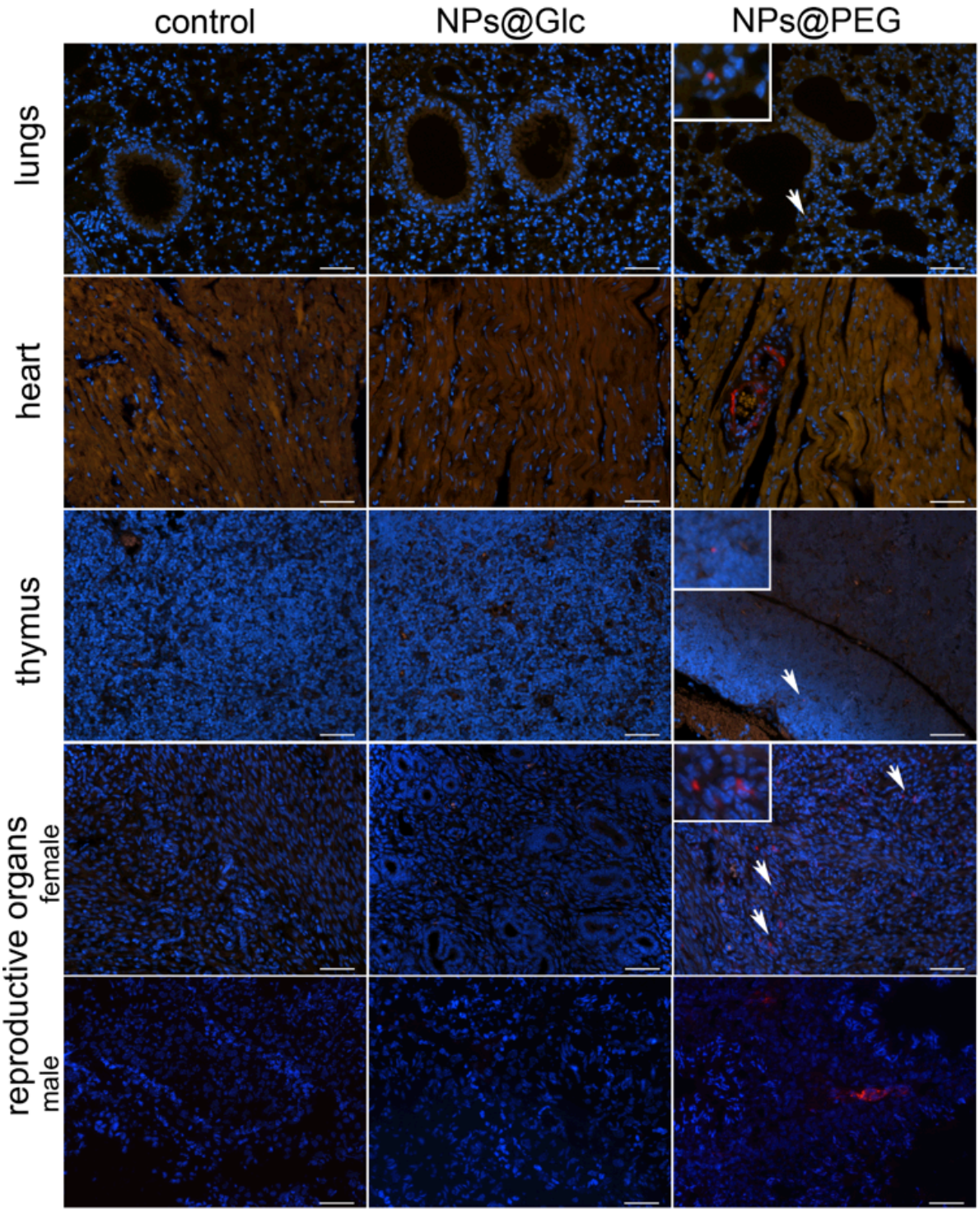

Figure S15. Biodistribution of NPs@Glc and NPs@PEG in mice lungs, heart, thymus and reproductive organs, analysed 72 h after NPs administration analyzed by fluorescence microscopy *ex vivo*. NPs@PEG have been detected in all of the mentioned organs, on the contrary to NPs@Glc. For

better visualization of NPs, fluorescence from red and green channels has been imposed. Scarcely accumulated NPs are indicated by white arrows and enlarged in the left upper corner of each corresponding image. Control tissue sections originate from PBS-treated mice. Cell nuclei were labeled with DAPI. Scale bar: 50 µm.

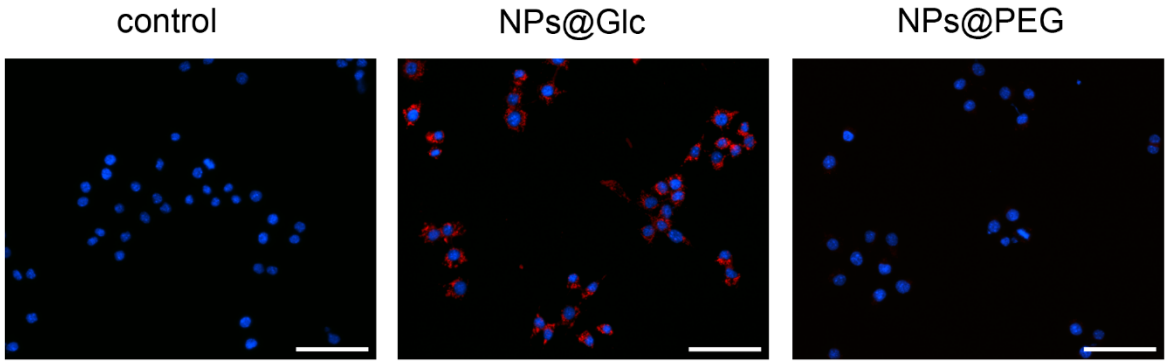

Figure S16. Uptake study of NPs@Glc and NPs@PEG bearing PC into mouse leukemic monocyte/macrophage cell line- RAW 264.7. After two hours of incubation in serum-free medium NPs@Glc were abundantly accumulated in the cells as intense red fluorescence was observed, whereas no uptake of NPs@PEG was detected. Cell nuclei were labeled with DAPI. Scale bar: 50 µm.

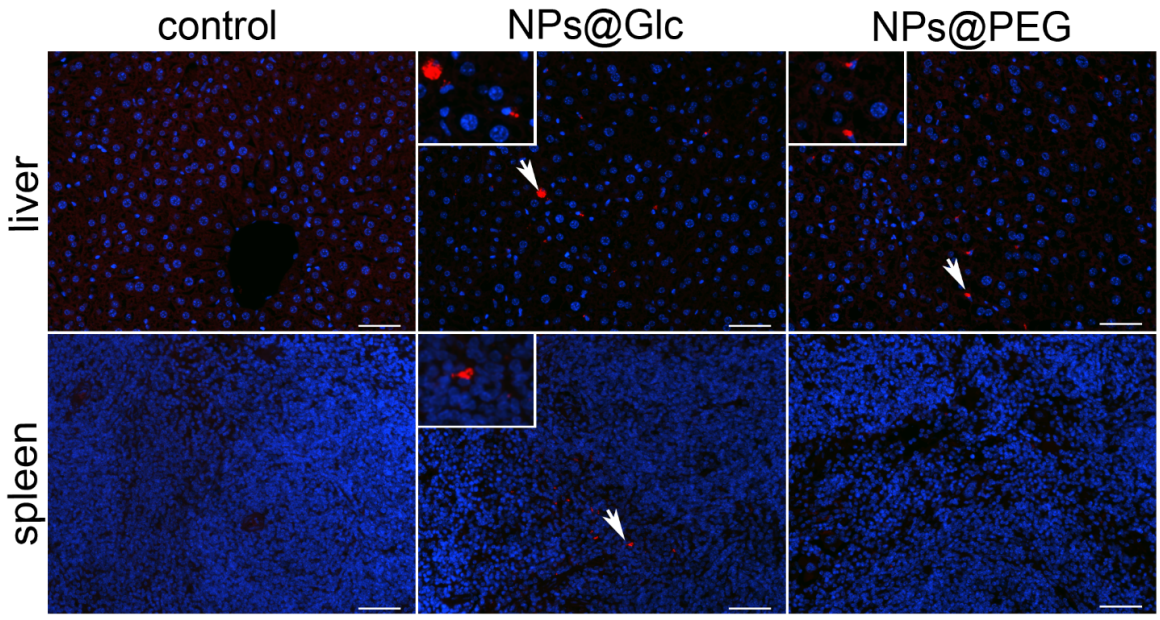

Figure S17. Biodistribution of NPs@Glc and NPs@PEG in mice liver and spleen tissues analyzed four months after NPs administration by fluorescence tissue examination *ex vivo*. NPs@Glc were found in the liver and spleen, whereas NPs@PEG only in the liver. Scale bar: 50 µm.

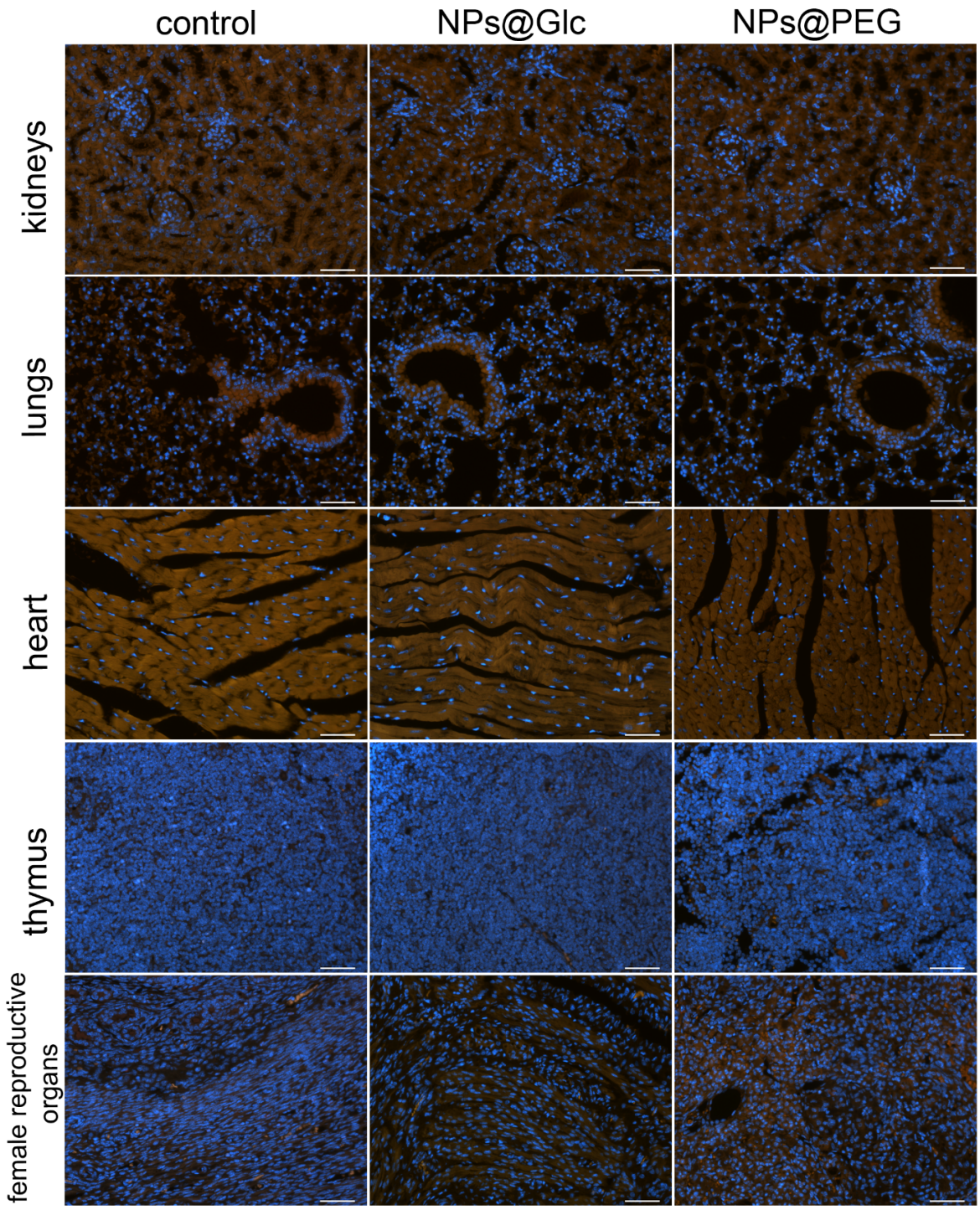

Figure S18. Biodistribution of NPs@Glc and NPs@PEG in mice kidneys, lungs, heart, thymus and reproductive organs, analysed four months after NPs administration by fluorescence microscopy *ex vivo*. Neither NPs@Glc nor NPs@PEG were detected in any of the mentioned organs. Scale bar: 50 µm.

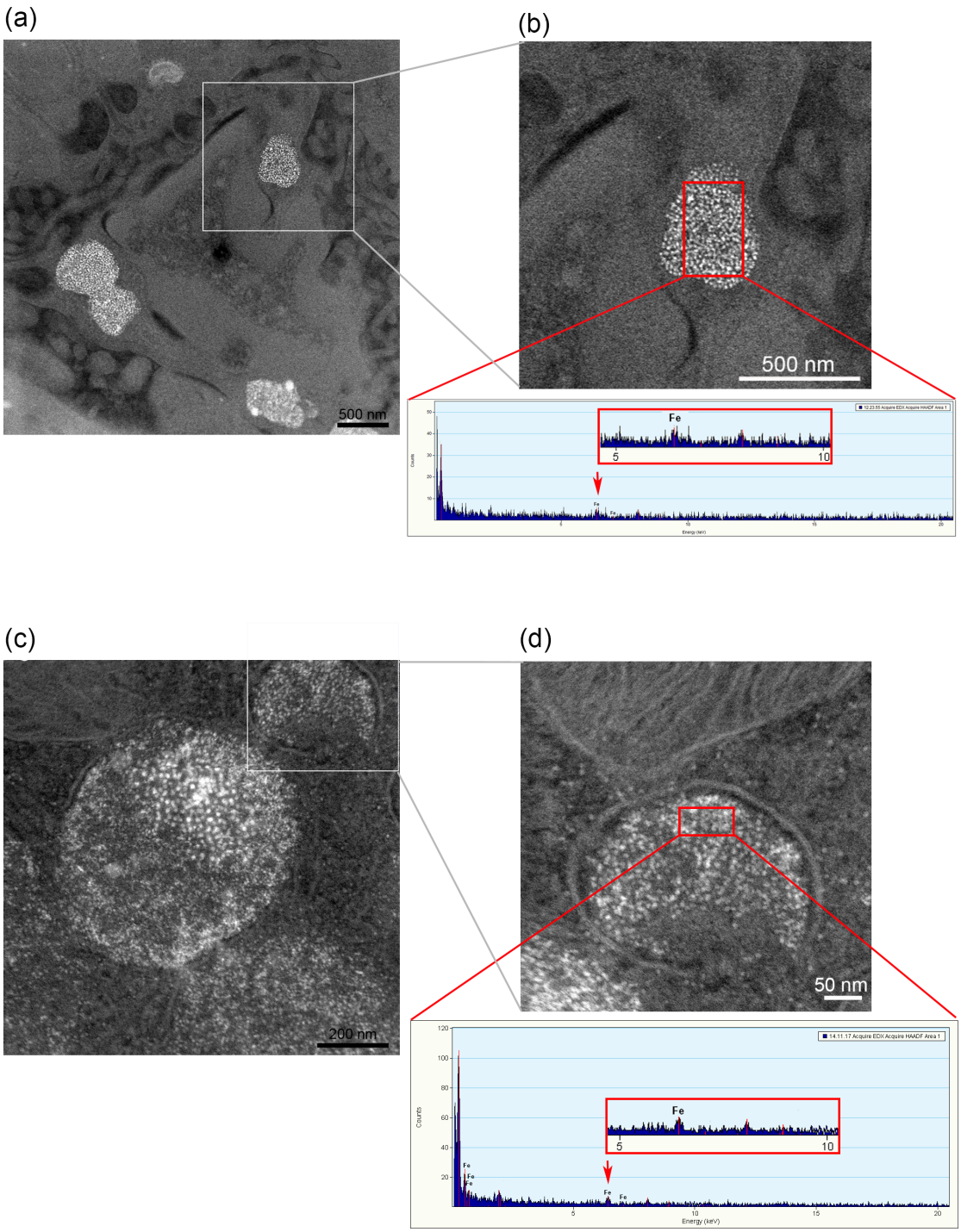

Figure S19. X-Ray Microanalysis (EDC) of NPs@Glc accumulated in the liver (a), (b) and spleen (c), (d) tissue. Areas restricted with white lines on micrographs (a) and (c) are enlarged on micrographs (b) and (d), respectively. The X-Ray Microanalysis spectrum corresponds to the areas restricted by red lines on micrographs (b) and (d). Iron peak corresponding to NPs is indicated by the red arrow and enlarged in a red-frame square.

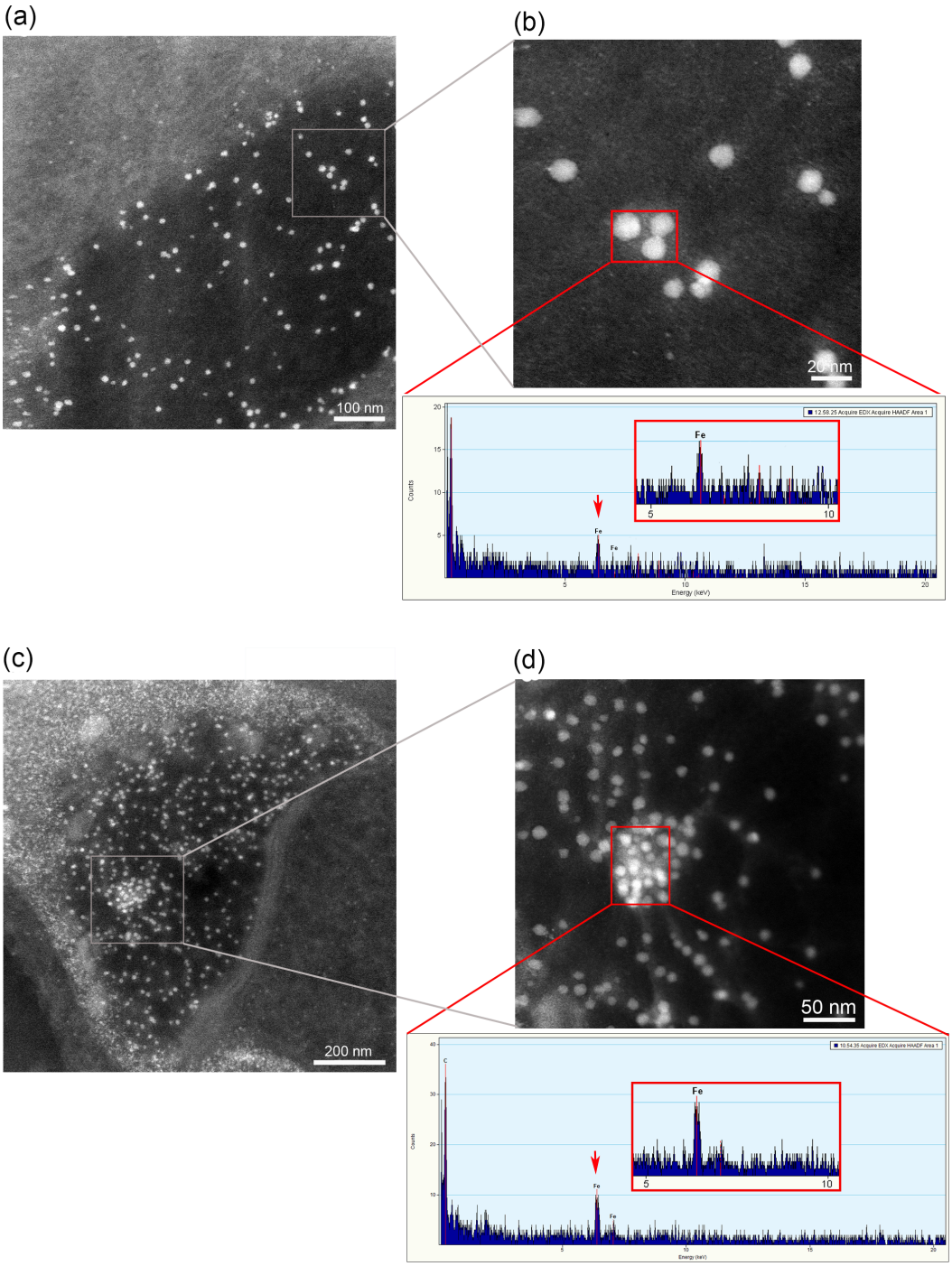

Figure S20. Ray Microanalysis (EDC) of NPs@PEG accumulated in the liver (a), (b) and spleen (c), (d) tissue. Areas restricted with white lines on micrographs (a) and (c) are enlarged on micrographs (b) and (d), respectively. The X-Ray Microanalysis spectrum corresponds to the areas restricted by red lines on micrographs (b)and (d). Iron peak corresponding to NPs is indicated by the red arrow and enlarged in a red-frame square.

References:

(1) Sun, S.; Zeng, H.; Robinson, D. B.; Raoux, S.; Rice, P. M.; Wang, S. X.; Li, G. Monodisperse MFe_2O_4 (M = Fe, Co, Mn) Nanoparticles. *J. Am. Chem. Soc.* **2004**, *126*, 273.

(2) Moros, M.; Pelaz, B.; López-Larrubia, P.; García-Martin, M. L.; Grazú, V.; de la Fuente, J. M. Engineering biofunctional magnetic nanoparticles for biotechnological applications. *Nanoscale* **2010**, *2*, 1746.

(3) Dias, J. T.; Moros, M.; del Pino, P.; Rivera, S.; Grazú, V.; de la Fuente, J. M. DNA as a molecular local thermal probe for the analysis of magnetic hyperthermia. *Angew. Chemie* **2013**, *125*, 11740.

(4) Chen, J.; Wang, H.; Long, W.; Shen, X.; Wu, D.; Song, S. S.; Sun, Y. M.; Liu, P. X.; Fan, S.; Fan, F.; Zhang, X. D. Sex differences in the toxicity of polyethylene glycol-coated gold nanoparticles in mice. *Int. J. Nanomedicine* **2013**, *8*, 2409.